Available online at www.sciencedirect.com
ScienceDirect
Trans. Nonferrous Met. Soc. China 34(2024) 2959−2971
Transactions of Nonferrous Metals Society of China
www.tnmsc.cn

Effect of sintering temperature and holding time on structure and properties of $Li_{1.5}Ga_{0.5}Ti_{1.5}(PO_4)_3$ electrolyte with fast ionic conductivity

Yin-yi LUO[1], Hao-zhang LIANG[1], Ping ZHANG[1], Lei HAN[2], Qian ZHANG[2], Li-dan LIU[1], Zhi-wei LUO[1], Tian-xiang NING[1], An-xian LU[1]

1. School of Materials Science and Engineering, Central South University, Changsha 410083, China;
2. School of Materials Science and Engineering, Jiangxi University of Science and Technology, Ganzhou 341000, China

Received 2 March 2023; accepted 23 February 2024

Abstract: $Li_{1.5}Ga_{0.5}Ti_{1.5}(PO_4)_3$ (LGTP) is recognized as a promising solid electrolyte material for lithium ions. In this work, LGTP solid electrolyte materials were prepared under different process conditions to explore the effects of sintering temperature and holding time on relative density, phase composition, microstructure, bulk conductivity, and total conductivity. In the impedance test under frequency of $1-10^6$ Hz, the bulk conductivity of the samples increased with increasing sintering temperature, and the total conductivity first increased and then decreased. SEM results showed that the average grain size in the ceramics was controlled by the sintering temperature, which increased from (0.54±0.01) μm to (1.21±0.01) μm when the temperature changed from 750 to 950 °C. The relative density of the ceramics increased and then decreased with increasing temperature as the porosity increased. The holding time had little effect on the grain size growth or sample density, but an extended holding time resulted in crack generation that served to reduce the conductivity of the solid electrolyte.

Key words: sintering temperature; holding time; conductivity; cracks; solid-state electrolyte

1 Introduction

Given the increasing energy demands and depletion of natural energy sources, the issue of energy storage has become a high global priority. Lithium-ion batteries have been widely studied as efficient energy conversion devices [1]. The commercial lithium-ion battery that uses liquid electrolytes exhibits a number of drawbacks, including leakage and combustion, low operating temperature, and instability at high temperatures and in humid, which severely hinder widespread application [2]. Consequently, all-solid-state lithium-ion batteries (ASSLB) are attracting appreciable research activity as a result of their high volumetric energy density, wide chemical compatibility, long cycle life, and high stability and safety [3]. The high Young's modulus of the solid electrolyte in ASSLBs hinders the dispersion of soluble materials in the electrode and inhibits the formation of lithium dendrites that can pierce the diaphragm, thereby improving the safety of the battery. The use of solid-state electrolytes (SSEs) enables the fabrication of light-weight, small size, and safer batteries [4]. Since the SSE serves as both separator and fast Li ion conductor, which largely determines battery performance, a significant research effort has been directed at developing solid electrolyte materials [5,6].

Corresponding author: Tian-xiang NING, Tel: +86-17775811033, E-mail: 308521225@qq.com;
An-xian LU, Tel: +86-13973136367, E-mail: axlu@mail.csu.edu.cn
DOI: 10.1016/S1003-6326(24)66588-X
1003-6326/© 2024 The Nonferrous Metals Society of China. Published by Elsevier Ltd & Science Press
This is an open access article under the CC BY-NC-ND license (http://creativecommons.org/licenses/by-nc-nd/4.0/)

Current research has largely focused on LISICON [7], chalcogenide [8], lithium phosphorous oxynitride, and NASICON [9] as potential SSEs. Although NASICON-type lithium titanium phosphate $LiTi_2(PO_4)_3$ (LTP) exhibits poor electrical conductivity, its internal structure can provide three-dimensional transport channels for lithium ions, which facilitate the improvement of electrical conductivity by ion doping. It was found that electrolyte conductivity was significantly increased by using trivalent cations (Al^{3+}, In^{3+}, Fe^{3+}, Cr^{3+}, and Sc^{3+}) to partially replace Ti^{4+} in $LiTi_2(PO_4)_3$ [10]. Trivalent doping of NASICON-type lithium titanium phosphate ($Li_{1+x}MIII_xMIV_{2-x}(PO_4)_3$) delivers high conductivity, a wide electrochemical window and enhanced stability in humid air, representing a SSE system that warrants further research and development [11]. The increased conductivity of doped $Li_{1+x}MIII_xMIV_{2-x}(PO_4)_3$ may be the result of a shorter lithium ion migration path distance, which serves to increase the ion concentration [12]. The $Li_{1+x}Al_xTi_{2-x}(PO_4)_3$ (LATP) obtained by substituting Ti^{4+} with Al^{3+} in LTP exhibits high ionic conductivity (10^{-4}−10^{-3} S/cm), stable chemistry, and enhanced mechanical strength [13]. Moreover, the density and grain size of the trivalent phosphate substituents is increased with increasing sintering temperature, accompanied by an increase in electrical conductivity. Therefore, it is necessary to explore the effects of different sintering temperatures and holding time on the structure and properties of SSEs, such as porosity, densification, grain and grain boundary size, phase composition, and micro-crack formation. Optimizations of these parameters are key to develop SSEs that deliver maximum performance. Few studies have addressed the effect of sintering temperature and holding time on the performance of LATP. MERTENS et al [14] investigated the effect of varying sintering temperature on the relative density and conductivity of LATP. XIAO et al [15] examined the dependence of conductivity for LATP SSE on holding time and sintering temperature. The results show that when the grain size is larger than a critical value (estimated as ca. 1.6 μm), a significant number of micro-cracks are generated [16,17]. These micro-cracks result in a rapid decrease in ionic conductivity, impacting SSE performance.

In addition to Al^{3+} substitution, other trivalent ions have also been investigated, such as Ga^{3+}, Ge^{3+}, and Y^{3+}. ZAJĄC et al [17] substituted Ti^{4+} with Ga^{3+} using a conventional high-temperature solid-phase method to prepare $Li_{1+x}Ga_xTi_{2-x}(PO_4)_3$. LIANG et al [18] prepared a thin film LGTP-Ga-20 mm solid-state electrolyte by using a hydrothermal method, achieving a conductivity of 2.3×10^{-4} S/cm. These findings suggest that LGTP can be used as a potential SSE [18,19]. The published studies have considered the effect of sintering methods on $Li_{1+x}Ga_xTi_{2-x}(PO_4)_3$ conductivity but did not explore the role of sintering temperature and holding time in determining the relationship between ionic conductivity and microscopic grain morphology. As mentioned above, the sintering temperature has a significant effect on the density, grain size, cracks, phase composition, and grain morphology of SSEs, whereas the holding time also affects the morphology and grain size of the particles. These features, in turn, affect SSE conductivity and should be carefully considered in developing viable LGTP systems.

In this study, we prepared LGTP electrolytes using a solid-phase method with varying sintering temperatures and investigated the effects of temperature on phase composition, relative density, microscopic morphology, grain size, total ionic conductivity, and bulk ionic conductivity of LGTP. In addition, the effects of holding time on the microscopic morphology, densities, and conductivity were examined at the optimal sintering temperature.

2 Experimental

2.1 Material synthesis

The experimental samples were first dried to remove any moisture. Then, the raw materials (Li_2CO_3, Ga_2O_3, TiO_2, and $NH_4H_2PO_4$) were weighed according to the stoichiometric ratios and placed in a ball mill container and ball milled in ethanol for 6 h. The resultant powder was heated to 400 °C for 4 h in air, subjected to a second ball milling for 6 h, followed by drying in an electric oven at 90 °C for 8 h. Before sintering, the LGTP precursor powder was added into appropriate amount of PVA to form fine particles and pressed at a fixed pressure of 25 MPa to obtain discs of 12 mm in diameter. The samples were sintered at

750, 800, 850, 900 and 950 °C for 6 h. The resultant materials are denoted as LGTP-750, LGTP-800, LGTP-850, LGTP-900, and LGTP-950, respectively. LGTP SSEs with sintering holding time of 2, 4, 6, 8, and 10 h at 800 °C were also prepared using the same procedure, and are denoted as LGTP-2, LGTP-4, LGTP-6, LGTP-8, and LGTP-10, respectively. Taking account of the volatilization of Li during sample preparation, 10% excess Li_2CO_3 was added in the synthesis process. The impedance test values of all the samples were obtained at 298 K.

2.2 Structural analysis

The phase composition of all the samples was examined using X-ray diffraction (XRD) with a scan speed of 8 (°)/min over the 10°−70° range. Measurements were conducted on a Bruker D500 using Bragg-Brentano configuration with Cu K_α radiation. The relative densities of the samples were obtained using deionized water as the medium, applying the Archimedean drainage method. Sample microstructure was determined by field emission scanning electron microscopy (SEM, Tescan Mira4 field emission scanning electron microscope, Czech Republic). The samples were analyzed in combination with an energy spectrum analyzer (EDS, X-max, Oxford Instruments) for elemental analysis.

2.3 Electrical performance

The electrochemical impedance spectra (EIS) of all samples were measured using a CHI660D electrochemical workstation (Shanghai Chenhua Equipment Co., Ltd., China) with a frequency range of 1 Hz to 1 MHz. The samples were polished before testing, recording the diameter and thickness before applying a uniform layer of silver paste to the upper and lower surfaces; stainless steel was used as a blocking electrode. In order to obtain the difference between the tested and fitted values, the impedance data were fitted using ZView software.

3 Results and discussion

3.1 Structural characterization

The XRD patterns of LGPT obtained by sintering at temperatures 750−950 °C are shown in Fig. 1. It can be seen that the intensity of the diffraction peaks increases with the increase of temperature, and the peaks for all the samples are consistent with those of the NASICON-type LTP (JCPDS No. 35-0754) pattern with the space group $R\bar{3}c$ [20].

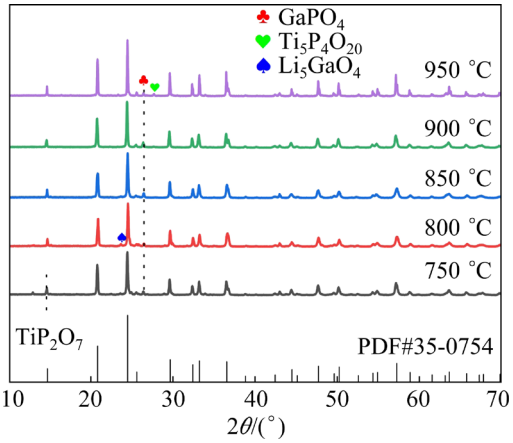

Fig. 1 XRD patterns of LGPT samples at different sintering temperatures

The main phase of the ceramic sample was formed at 750 °C, and a small amount of TiP_2O_7 impurity phase was generated. An increase of temperature to 900 °C results in the $GaPO_4$ impurity phase. This is probably due to the substitution of Ti^{4+} by Ga^{4+}, leading to the formation of $GaPO_4$ by combining the interstitial Ga ions from the LGTP lattice with PO_4^{3-} [21]. When the temperature exceeds 900 °C, the formation of another impurity phase ($Li_5P_4O_{20}$) is a feature of LATP [22].

The SEM images of LGTP ceramics generated at different temperatures and the corresponding grain size histograms are presented in Figs. 2(a−e). It can be seen that the ceramics prepared below 850 °C exhibit a dense structure. This may be due to the fact that after treating the powder at 400 °C for 4 h, the LGTP particles become finer and homogeneous, which facilitates the formation of dense ceramic particles. The samples exhibited a regular cubic shape with close contact between particles and no obvious cracks. As the sintering temperature increases, the particle size of the sample increases; at 750−800 °C, the samples exhibited particle sizes in the range of 0.45−0.75 μm, with some sizes exceeding 1 μm. As the temperature was raised to 850 °C, the particles showed a larger size and different shapes. A further increase in temperature resulted in a particle size in the range of 0.9−1.3 μm, demonstrating particle

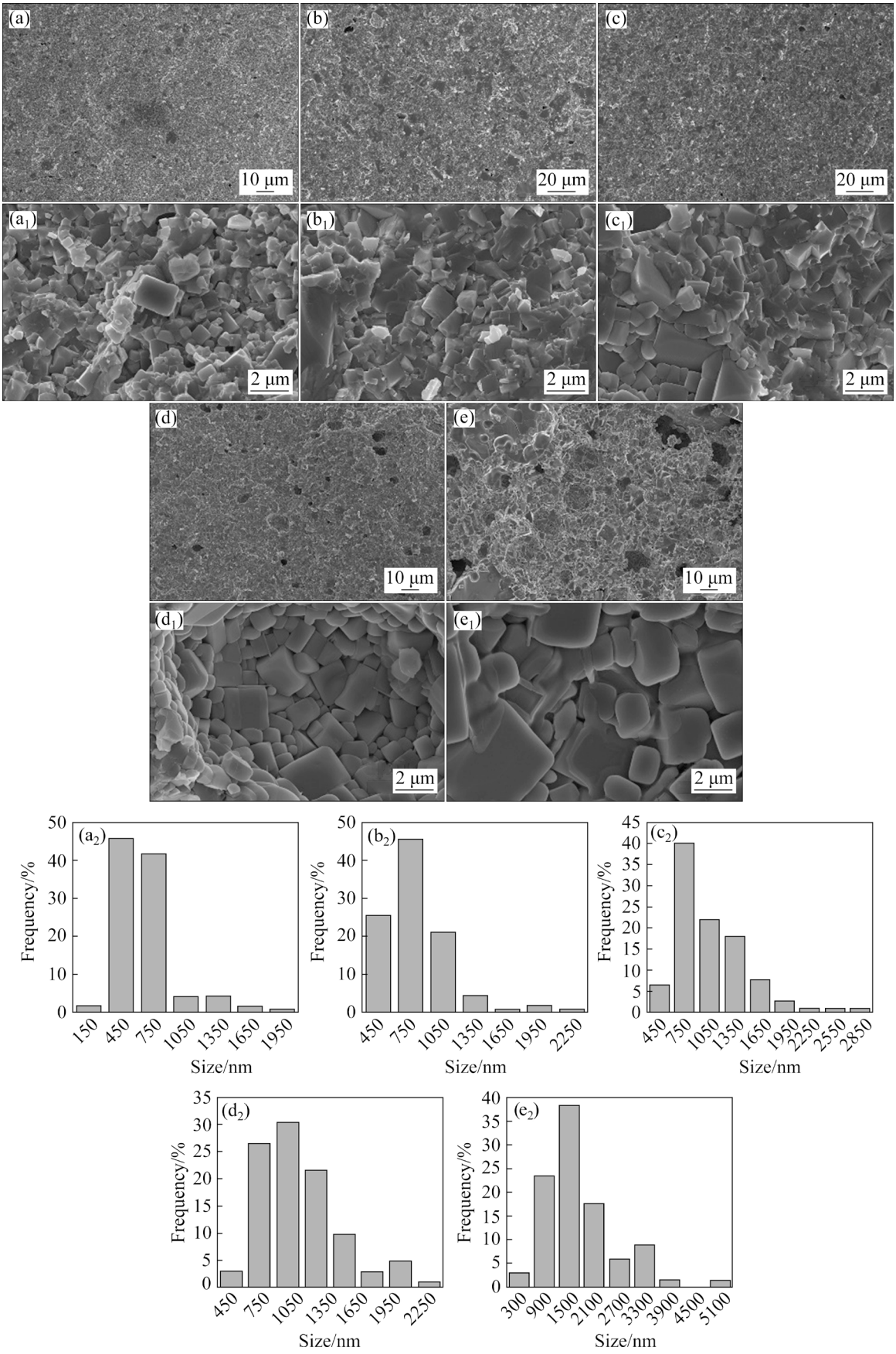

Fig. 2 SEM images of LGTP at different calcination temperatures, and corresponding particle size histograms: (a, a_1, a_2) 750 °C; (b, b_1, b_2) 800 °C; (c, c_1, c_2) 850 °C; (d, d_1, d_2) 900 °C; (e, e_1, e_2) 950 °C

growth. Moreover, the better contact between grains results in a facilitated Li^+ diffusion between the tightly packed grains. The relative densities of the LGTP-750, LGTP-800, LGTP-850, LGTP-900, and LGTP-950 samples were calculated using the Archimedes' principle, giving values of 91.2%, 96.4%, 94.2%, 88.7%, and 85.6%, respectively. An increase in sintering temperature is accompanied by an initial increase and subsequent decrease in relative density. When the temperature exceeds 850°C, the resultant generated by volatilization pores help to reduce sample density.

Figure 3(a) represents the SEM image of ceramic samples sintered at 800 °C for 6 h while Fig. 3(b) shows the EDS result of LGTP-800. It can be seen that the sample consists of Li, Ga, Ti, P, and O elements, and the associated elemental contents are close to the nominal values. Indeed, a combination of EDS elemental mapping and area scan results in an elemental content close to $Li_{1.5}Ga_{0.5}Ti_{1.5}(PO_4)_3$.

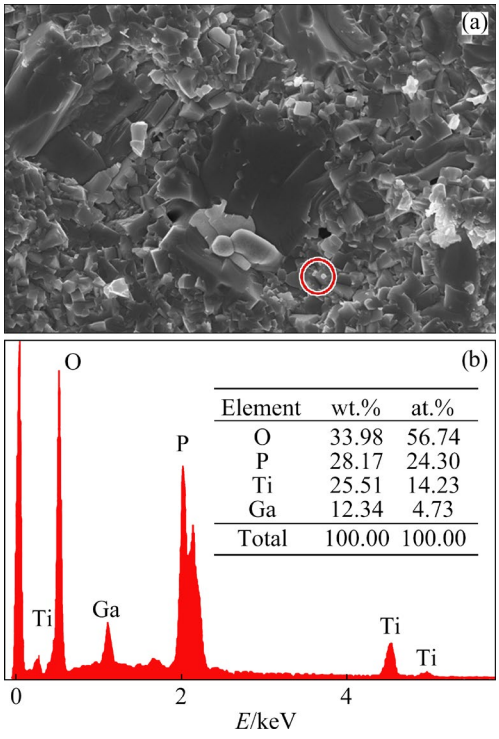

Fig. 3 SEM image of sample sintered at 800 °C for 6 h (a), and EDS spectrum of $Li_{1.5}Ga_{0.5}Ti_{1.5}(PO_4)_3$ (b)

3.2 Conductivity analysis

An important factor in determining superior performance of solid electrolytes is ionic conductivity [23]. Impedance tests were performed on the LGTP SSEs ceramics obtained after sintering at 750−950 °C, and the results are shown in Fig. 4(a) for samples tested in the frequency range of 1−10^6 Hz. The resultant Nyquist plots, based on the equivalent circuit selected for the experiments and application of ZView software, exhibit a semicircle at high frequencies and an inclined straight line at low frequencies. The semicircle associated with the bulk resistance (R_b) of the solid electrolyte is observed at measurements greater than 10^6 Hz, which is beyond the operating frequency of the electrochemical workstation [24]. Nevertheless, the origin of the semicircle can be used as a measure of bulk resistance, and is taken as an approximation of R_b in the equivalent circuit chosen in this study. The parameter R_{gb} in parallel with the first constant phase element (CPE_1) corresponds to the semicircle and represents the grain boundary resistance (R_{gb}) [25], whereas the second parameter (CPE_2) corresponds to the straight line, representing the electrolyte and Pt blocking electrode with respect to Li^+ transfer resistance; the total resistance is represented by $R_t=R_{gb}+R_b$.

It can be seen in Fig. 4(a) that the semicircle decreases in intensity as the sintering temperature rises from 750 to 800 °C. A further increase in temperature results in an increased intensity where the LGTP-800 sample generates the smallest semicircle. The AC impedance spectrum of the LGTP-800 sample, which showed the lowest total resistance about 1607 Ω was investigated further, and the results are presented in Fig. 4(b). As the temperature increases, the grain resistance shows an initial decrease with increasing temperature while a subsequent increase in grain boundary resistance at temperatures in excess of 400 °C. The sample bulk conductivity (σ_b) and total conductivity (σ_t) can be calculated using the following equation:

$$\sigma=\frac{H}{RS} \tag{1}$$

where σ, H, R, and S denote the conductivity, thickness, resistance, and effective area of the solid electrolyte, respectively. The relative density, activation energy, bulk resistance, grain boundary resistance, and total conductivity of the samples sintered at different temperatures are listed in Table 1. The total conductivity of the samples and the equivalent circuit used to fit the impedance spectra are given in Figs. 4(d) and (e), respectively.

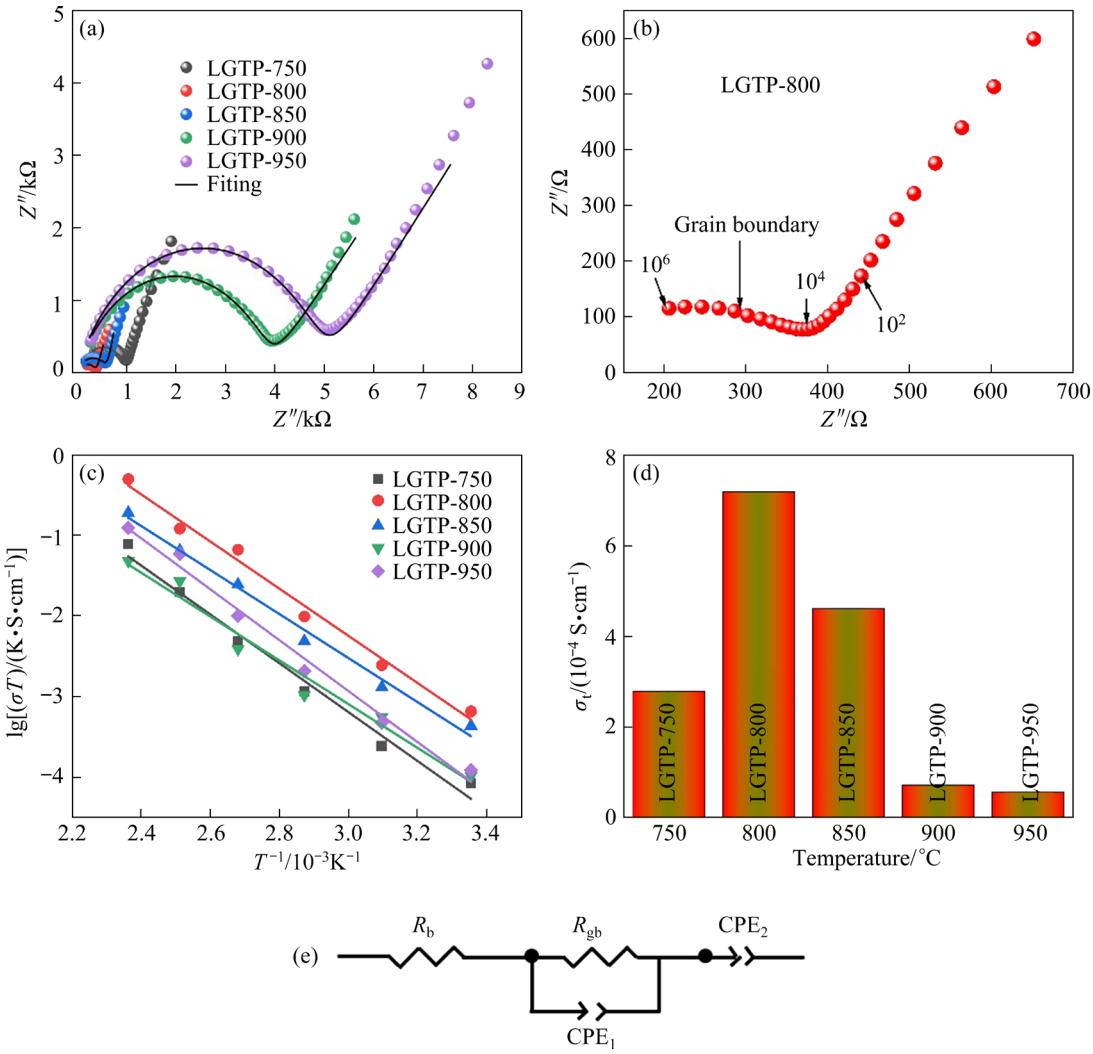

Fig. 4 Nyquist plots and fitted curves for samples sintered at different temperatures (a), Nyquist plot for LGTP-800 (b), Arrhenius plots of LGTP-750, LGTP-800, LGTP-850, LGTP-900 and LGTP-950 (c), total conductivity (d), and equivalent circuit used to fit impedance spectra (e)

Table 1 Relative density, activation energy (E_a), bulk conductivity (σ_b), grain boundary conductivity (σ_{gb}) and total conductivity (σ_t) for LGTP-750, LGTP-800, LGTP-850, LGTP-900 and LGTP-950 measured at room temperature

Sample	Relative density/%	E_a/eV	σ_b/(S·cm^{-1})	σ_{gb}/(S·cm^{-1})	σ_t/(S·cm^{-1})
LGTP-750	91.2	0.21	1.38×10^{-3}	2.95×10^{-4}	2.79×10^{-4}
LGTP-800	96.4	0.20	1.76×10^{-3}	7.59×10^{-4}	7.19×10^{-4}
LGTP-850	94.2	0.23	1.89×10^{-3}	4.76×10^{-4}	4.62×10^{-4}
LGTP-900	88.7	0.27	2.02×10^{-3}	7.43×10^{-5}	7.28×10^{-5}
LGTP-950	85.6	0.29	3.11×10^{-3}	5.84×10^{-5}	5.67×10^{-5}

As shown in Table 1, the grain boundary conductivity and total conductivity increase and then decrease with temperature, where LGTP-800 exhibited the largest grain boundary conductivity (7.59×10^{-4} S/cm) and total conductivity (7.19×10^{-4} S/cm). The total conductivity of LGTP-800 is comparable to values reported in the literature for electrolytes prepared using other methods [26]. It should be noted that the grain boundary conductivity determines the total conductivity when the presence of pores and micro-cracks are not considered, which serves to

indicate that the grain boundary resistance plays an important role in the total resistance of doped LTP. The total conductivity of the LGTP electrolyte samples adheres to the Arrhenius equation:

$$\sigma T = A\exp\left(\frac{-E_a}{K_B T}\right) \quad (2)$$

where σ represents the total conductivity, A is the pre-exponential term, K_B is the Boltzmann constant, E_a is the activation energy of the electrolyte, and T represents the temperature. The associated Arrhenius plots are shown in Fig. 4(c). The activation energy of the electrolyte particles can be calculated from the slope of the Arrhenius plot, giving values of 0.21, 0.20, 0.23, 0.27, and 0.29 eV for LGTP-750, LGTP-800, LGTP-850, LGTP-900, and LGTP-950, respectively.

Based on the above analysis, it can be seen that LGTP-800 exhibits the highest total conductivity which can be attributed to the following features: (1) As the temperature increases from 750 to 800 °C, grain growth is promoted, the number of grain boundaries is reduced, the grain boundary conductivity increased, and the total conductivity is also increased. (2) According to related studies, an electrolyte with high ionic conductivity must also have a high density [27], where LGTP-800 exhibits the highest relative density (Fig. 4(d)). (3) An increase in temperature promotes the growth of grain size, resulting in a decrease in the number of grain boundaries. The total conductivity decreases with further increase in sintering temperature from 850 to 950 °C. Although the number of grain boundaries decreases, the increase in the number of pores and the enlargement of pores at high temperatures prevent the migration of Li ions in the pores, both macroscopically and microscopically, resulting in a decrease in conductivity. This can be verified from the entries in Figs. 2(d) and (e), suggesting that the effect of porosity on conductivity is greater than that of grain boundaries. (4) LGTP-800 has a high crystallinity with a small secondary phase component that ensures the integrity of the NASICON structure in facilitating lithium-ion transport. Moreover, the generation of a Li_5GaO_4 impurity phase also can promote the conductivity [28]. (5) The lowest activation energy recorded for LGTP-800 indicates lower energy requirements for the migration of lithium ions with a consequent enhancement of conductivity [29].

The bulk conductivity is an inherent property of the material determined by the composition of the material itself and should not be affected by temperature. However, as shown in Table 1, the grain conductivity increases with increasing temperature. This indicates that the composition and crystallinity of LGTP is temperature dependent, as noted elsewhere $Li_{1.5}Al_{0.5}Ti_{1.5}(PO_4)_3$. The rate of ion diffusion inside the grains is related to the long-range order of the material, which is determined by sample crystallinity. The crystallinity of the LGTP samples can be determined by XRD analysis with an estimation of particle size based on the full width at half maximum (FWHM) of the (113) peak at a 2θ of 24.44°.

The relationship between the FWHM and temperature, shown in Fig. 5(a), reveals an inverse proportionality. The associated XRD peak exhibits an increased sharpness with increasing temperature (Fig. 5(c)), indicating that the crystallinity increases. In addition, an increase in temperature induces faster diffusion of ions and an increase in the rate of particle-to-particle fusion resulting in the formation of larger grains. This results in the generation of samples with higher long-range order and greater crystallinity. The sample treated at 950 °C exhibits enhanced crystallinity with the lowest FHWM (0.121°).

The relationship between bulk ionic conductivity and FWHM is shown in Fig. 5(b), where it can be seen that the higher the crystallinity the faster the diffusion of ions and the greater the value of bulk ionic conductivity, reaching a value of 3.11×10^{-3} S/cm in the case of LGTP-950. This is significantly higher than the bulk conductivity of LGTP (10^{-4} S/cm). In addition, a comparison may be made from the entries in Table 2 with other doping ions used to modify the conductivity of related systems. It can be seen that the LGPT conductivity achieved in this study is higher than that recorded previously.

3.3 Effect of holding time on electrical properties

As noted above, the sintering time has the same effect on LGTP phase composition, micromorphology, and electrical conductivity. The effect of different holding time at 800 °C on the electrolyte properties of ceramic was investigated,

and the resultant XRD patterns are shown in Fig. 6(c).

The $GaPO_4$ impurity is present in all the samples, which can serve to increase sample density. The sharpness of the XRD peaks indicates a high level of crystallinity due to sintering [35], and all samples match the NASICON ($LiTi_2(PO_4)_3$) reference. The relationship between FWHM and holding time is shown in Fig. 6(a), and the crystallinity of the sample remains basically. The dependence of bulk ionic conductivity on FWHM is presented in Fig. 6(b). The relative density, volume, grain boundaries, and total conductivity of the samples are given in Table 3.

It can be seen that the grain resistance decreased with an initial increase in holding time (from 2−6 h), and subsequently increased with increasing holding time. The bulk ionic conductivity reached the maximum of 1.8×10^{-3} S/cm at a holding time of 6 h. Compared with the volumetric conductivities obtained at other holding time at a fixed temperature has revealed that the differences in grain conductivity are not significant. This phenomenon indicates that the holding time has little effect on crystallinity or grain size.

The AC impedance spectra of LGTP-2, LGTP-4, LGTP-6 LGTP-8, and LGTP-10 are shown in Fig. 7(a). All the samples generate a semicircle

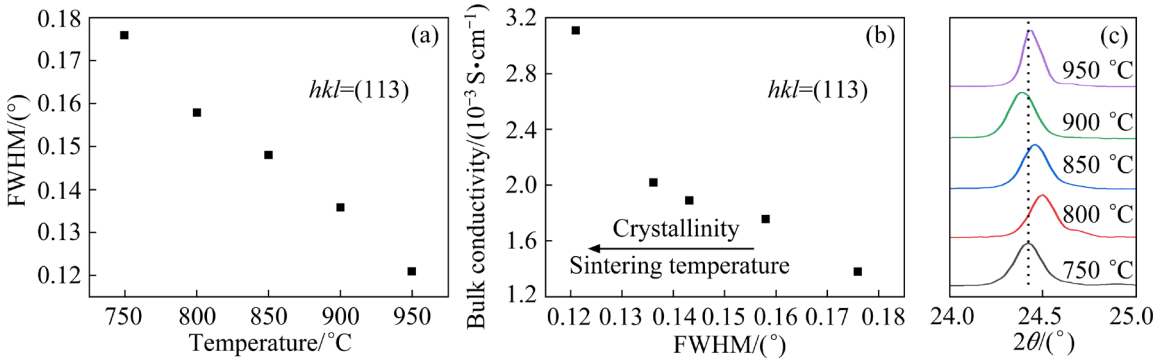

Fig. 5 FWHM of (113) XRD peak as function of sintering temperature (a), bulk conductivity as function of FWHM (crystallinity) (b), and temperature dependence of (113) XRD peak (c)

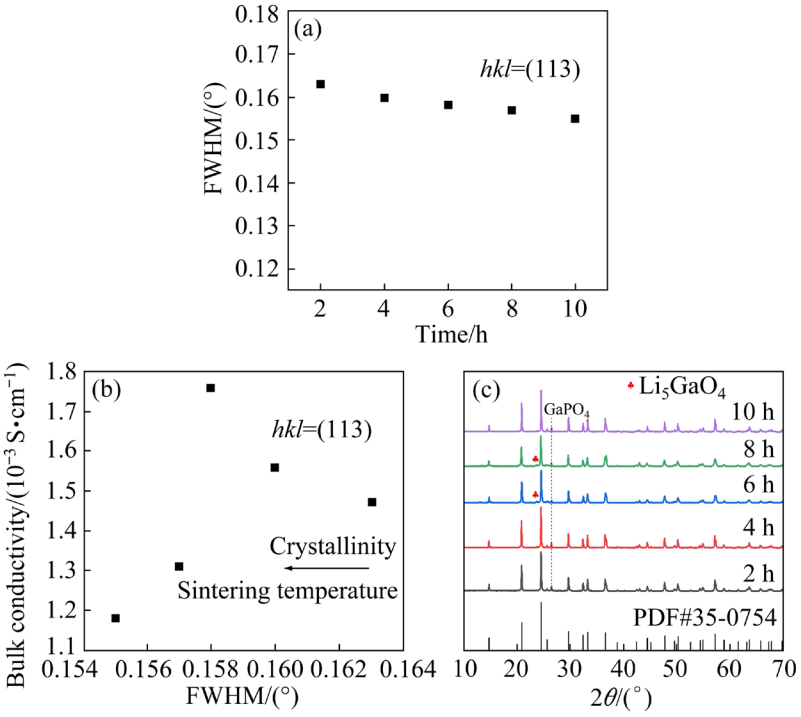

Fig. 6 Plot of FWHM as function of holding time (a), plot of bulk conductivity versus FWHM (b), and XRD patterns of LGPT samples sintered at 800 °C with different holding time (c)

Table 2 Comparison of conductivity of different trivalent ion doped LTPs

Sample	σ_t/(10^{-4} S·cm^{-1})	Testing temperature/K	Preparation method
$Li_{1.4}Al_{0.4}Ti_{1.6}(PO_4)_3$	5.4	298	Sol−gel method [30]
$Li_{1.5}Al_{0.5}Ti_{1.5}(PO_4)_3$	2.3	298	Solid phase method [31]
$Li_{1.3}Al_{0.3}Te_{0.03}Ti_{1.67}(PO_4)_3$	7.03	473	Solid phase method [32]
$Li_{1.5}Al_{0.5}Ge_{1.5}(PO_4)_3$	1.6	303	Hydrothermal-assisted solid phase method [33]
$Li_{1.6}Ti_{1.5}Fe_{0.4}Ca_{0.1}(PO_4)_3$	2.66	298	Solid phase method [34]
$Li_{1.5}Ga_{0.5}Ti_{1.5}PO_4$	7.2	298	Solid phase method (This work)

Table 3 Relative density, bulk conductivity (σ_b), grain boundary conductivity (σ_{gb}) and total conductivity (σ_t) of LGTP-2, LGTP-4, LGTP-6, LGTP-8 and LGTP-10 measured at 298 K

Sample	σ_b/(10^{-3} S·cm^{-1})	σ_{gb}/(10^{-4} S·cm^{-1})	σ_t/(10^{-4} S·cm^{-1})	Relative density/%
LGTP-2	1.47	2.07×	1.94	95.8
LGTP-4	1.56	2.98	2.64	96.1
LGTP-6	1.8	7.59	7.19	96.5
LGTP-8	1.31	4.8	4.66	96.3
LGTP-10	1.18	0.346	0.27	96.7

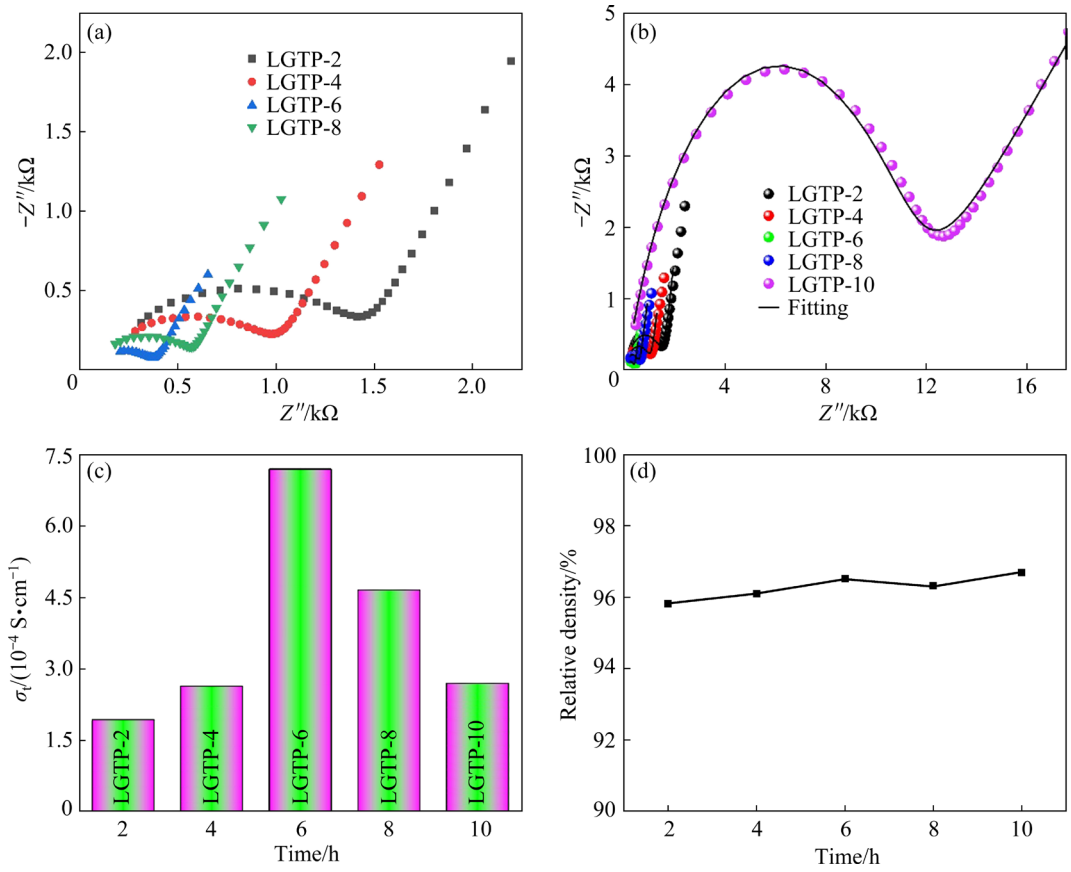

Fig. 7 Amplified impedance diagram (a), impedance of samples sintered at 800 °C with different holding time (b), total conductivity as function of holding time (c), and relative density with different holding time (d)

response from high to medium frequencies with a linear dependency at low frequencies. As shown in Fig. 7(b), LGTP-6 exhibits the smallest semicircle, suggesting the lowest total resistance. The relative density is plotted as a function of holding time in Fig. 7(d), where it can be seen that all the prepared

samples have high relative densities.

The level of densification is largely unaffected by holding time, and grain size does not change significantly with extended holding time. However, at a holding time in excess of 8 h, micro-cracks are observed on the grain surface, which can seriously hinder the diffusion of lithium ions and lower the electrolyte conductivity. Micro-cracking is the result of material anisotropy and the possible mechanical stresses that occur during cooling over a longer holding time [36]. The total conductivity is presented as a function of holding time in Fig. 7(c), where an initial increase is evident (between 2 and 6 h), followed by a sharp decrease. Representative SEM images of the sample obtained by sintering at different holding time are shown in Fig. 8. It can be seen that the grains are uniformly distributed with an average grain size of (1.1±0.4) μm. The images reveal a close connection between the grains, and a rather dense microstructure with no obvious holes or voids.

The LGTP-6 sample exhibits the highest total conductivity about 7.19×10^{-4} S/cm for a holding time of 6 h. Sample conductivity is essentially constant for a holding time in the range of 2−4 h, consistent with the invariance of grain size, crystallinity, and phase composition. An increase in holding time from 4 to 6 h is accompanied by an increase in conductivity due to the generation of the conductive Li_5GaO_4 phase. The observed decrease in conductivity when the holding time is extended to 8 h can be attributed to grain cracking, which inhibits the diffusion of lithium ions. Sample anisotropy results in crack formation as a result of prolonged holding time followed by excessive mechanical stress during the cooling process [37]. At a holding time of 10 h, total conductivity exhibits a marked decrease due to the presence of cracks and pores, while the density of sample reached a maximum.

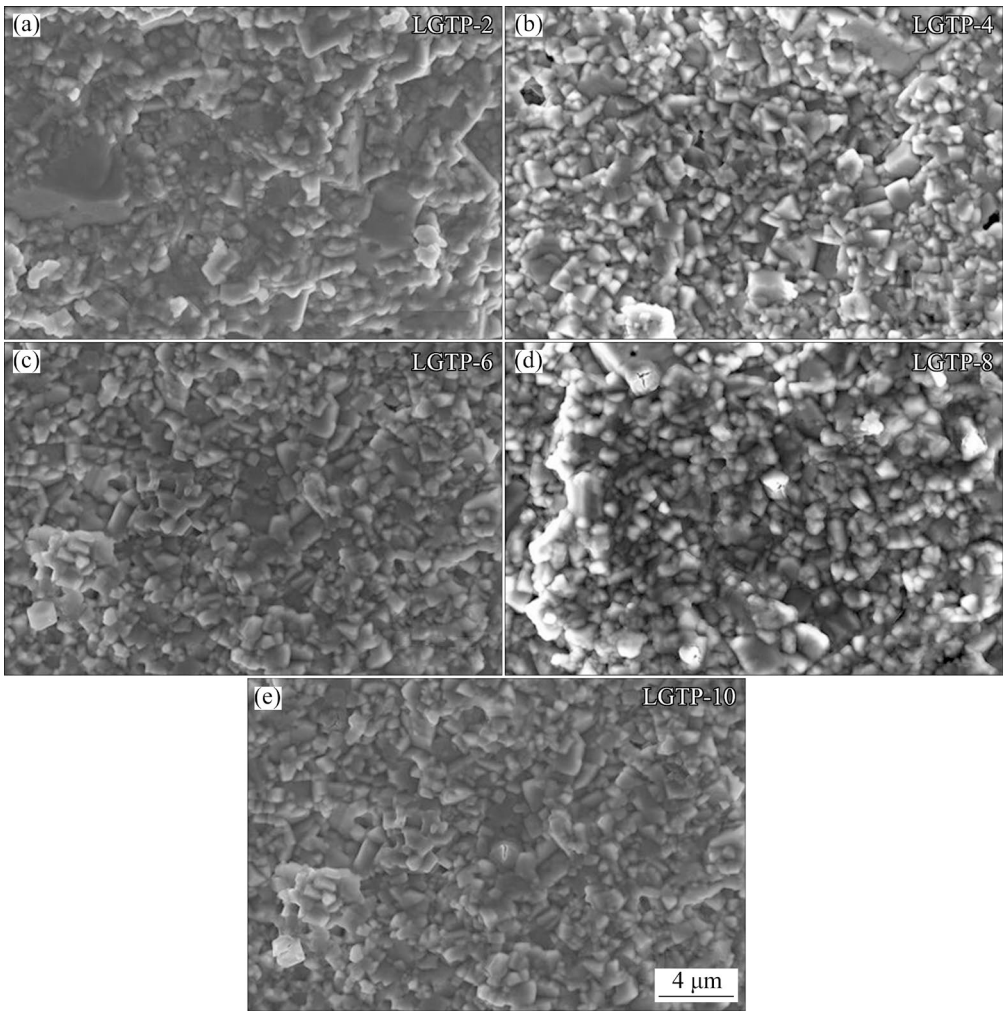

Fig. 8 SEM images of samples sintered at 800 °C with different holding time

4 Conclusions

(1) The total conductivity of LGTP solid electrolytes exhibited an initial increase and subsequent decrease with the increase of sintering temperature, and the bulk conductivity increased with the increase of temperature to reach a maximum of 7.19×10^{-4} S/cm when the sample was sintered at 800 °C.

(2) The relative density and average grain size of LGTP samples increased with increasing sintering temperature, which served to enhance conductivity.

(3) The holding time has little effect on sample crystallinity and grain size, but a prolonged holding time can lead to the formation of cracks, which have a detrimental effect on electrical conductivity.

CRediT authorship contribution statement

Yin-yi LUO: Conceptualization, Methodology, Formal analysis, Funding acquisition; **Hao-zhang LIANG:** Conceptualization, Methodology, Formal analysis; **Ping ZHANG:** Investigation, Writing − Original draft; **Lei HAN:** Investigation, Writing − Original draft; **Qian ZHANG:** Formal analysis, Data curation, Writing − Review & editing; **Li-dan LIU:** Supervision, Formal analysis; **Zhi-wei LUO:** Formal analysis, Data curation, Validation; **Tian-xiang NING:** Supervision, Writing − Review & editing; **An-xian LU:** Supervision, Conceptualization, Investigation, Writing − Review & editing.

Declaration of competing interest

The authors declare that they have no known competing financial interests or personal relationships that could have appeared to influence the work reported in this paper.

Acknowledgments

The work was funded by the National Natural Science Foundation of China (Nos. 51672310, 51272288, 51972344).

References

[1] GUO Zhi-hao, LI Xin-hai, WANG Zhi-xing, GUO Hua-jun, PENG Wen-jie, HU Qi-yang, YAN Guo-chun, WANG Jie-xi. Empirical decay relationship between ionic conductivity and porosity of garnet type inorganic solid-state electrolytes [J]. Transactions of Nonferrous Metals Society of China, 2022, 32(10): 3362−3373.

[2] CAI Hong, YU Tong, XIE Dong-rui, SUN Ben-shuang, CHENG Jiang, LI Lu, BAO Xu-jin, ZHANG Hong-tao. Microstructure and ionic conductivities of NASICON-type $Li_{1.3}Al_{0.3}Ti_{1.7}(PO_4)_3$ solid electrolytes produced by cold sintering assisted process [J]. Journal of Alloys and Compounds, 2023, 939: 168702.

[3] LI Cheng-feng, MURUGANANTHAM R, HSU W C, IHRIG M, HSIEH C T, WANG C C, LIU Wei-ren. Atomic layer deposition of ZnO on $Li_{1.3}Al_{0.3}Ti_{1.7}(PO_4)_3$ enables its application in all solid-state lithium batteries [J]. Journal of the Taiwan Institute of Chemical Engineers, 2023, 144: 104681.

[4] SHEN Shao-peng, TANG Geng, LI Hong-ji, ZHANG Liang, ZHENG Jin-chi, LUO Yuan, YUE Jun-pei, SHI Yong-zheng, CHEN Zhe. Low-temperature fabrication of NASICON-type LATP with superior ionic conductivity [J]. Ceramics International, 2022, 48(24): 36961−36967.

[5] YU Qing-jiang, JIANG Ke-cheng, YU Cui-ling, CHEN Xian-jin, ZHANG Chuan-jian, YAO Yi, JIANG Bin, LONG Hui-jin. Recent progress of composite solid polymer electrolytes for all-solid-state lithium metal batteries [J]. Chinese Chemical Letters, 2021, 32(9): 2659−2678.

[6] ISHII K, UCHIKOSHI T, MIYOSHI S, ODE M, OHNO T, TAKADA K. Reactivity evaluation of NASICON-type solid electrolyte LATP, LAGP and Olivine-type cathode LCP [J]. Materials Letters, 2022, 324: 132736.

[7] JUN K J, SUN Ying-zhi, XIAO Yi-han, ZENG Yan, KIM R, KIM H, MIARA L J, IM D, WANG Yan, CEDER G. Lithium superionic conductors with corner-sharing frameworks [J]. Nature Materials, 2022, 21: 924−931.

[8] YANG Tian-qi, WANG Cheng, ZHANG Wen-kui, XIA Yang, HUANG Hui, GAN Yong-ping, HE Xin-ping, XIA Xin-hui, TAO Xin-yong, ZHANG Jun. A critical review on composite solid electrolytes for lithium batteries: Design strategies and interface engineering [J]. Journal of Energy Chemistry, 2023, 84:189−209.

[9] PAN Ke-cheng, LI Ming-hui, WANG Wei-cheng, XING Shuo-chao, DOU Ya-ying, GAO Sha-sha, ZHANG Zhang, ZHOU Zhen. A leap by the rise of solid-state electrolytes for Li-air batteries [J]. Green Energy & Environment, 2023, 8(4): 939−944.

[10] ZHAO Xiang-chao, LUO Yuan-song, ZHAO Xiu-jian. Effect of TeO_2 sintering aid on the microstructure and electrical properties of $Li_{1.3}Al_{0.3}Ti_{1.7}(PO_4)_3$ solid electrolyte [J]. Journal of Alloys and Compounds, 2022, 927: 167019.

[11] CHEN Shu-yu, HSIEH C T, ZHANG Ren-shuo, MOHANTY D, GANDOMI Y A, HUNG I M. Hybrid solid state electrolytes blending NASICON-type $Li_{1+x}Al_x$-$Ti_{2-x}(PO_4)_3$ with poly (vinylidene fluoride-co-hexafluoropropene) for lithium metal batteries [J]. Electrochimica Acta, 2022, 427: 140903.

[12] JIN Ying-min, LIU Chao-jun, ZONG Xin, LI Dong, FU Meng-yu, TAN Si-ping, XIONG Yue-ping, WEI Jun-hua. Interface engineering of $Li_{1.3}Al_{0.3}Ti_{1.7}(PO_4)_3$ ceramic electrolyte via multifunctional interfacial layer for all-solid-state lithium batteries [J]. Journal of Power Sources, 2020, 460: 228125.

[13] VIEIRA E M F, RIBEIRO J F, SILVA M M, BARRADAS N P, ALVES E, ALVES A, CORREIA M R, GONCALVES L M. Electrical insulation properties of RF-sputtered LiPON layers towards electrochemical stability of lithium batteries [J]. Journal of Physics D: Applied Physics, 2016, 49: 485301.

[14] MERTENS A, YU Shi-cheng, SCHÖN N, GUNDUZ D C, TEMPEL H, SCHIERHOLZ R, HAUSEN F, KUNGL H, GRANWEHR J, EICHEL R A. Superionic bulk conductivity in $Li_{1.3}Al_{0.3}Ti_{1.7}(PO_4)_3$ solid electrolyte [J]. Solid State Ionics, 2017, 309: 180−186.

[15] XIAO Wei, WANG Jing-yu, FAN Lin-lin, ZHANG Jiu-jun, LI Xi-fei. Recent advances in $Li_{1+x}Al_xTi_{2-x}(PO_4)_3$ solid-state electrolyte for safe lithium batteries [J]. Energy Storage Materials, 2019, 19: 379−400.

[16] JACKMAN S D, CULTER R A. Effect of microcracking on ionic conductivity in LATP [J]. Journal of Power Sources, 2012, 218: 65−72.

[17] ZAJĄC W, TARACH M, TRENCZEK-ZAJĄC A. Towards control over redox behaviour and ionic conductivity in $LiTi_2(PO_4)_3$ fast lithium-ion conductor [J]. Acta Materialia, 2017, 140: 417−423.

[18] LIANG Yan-jie, PENG Cong, KAMIIKE Y, KURODA K, OKIDO M. Gallium doped NASICON type $LiTi_2(PO_4)_3$ thin-film grown on graphite anode as solid electrolyte for all solid state lithium batteries [J]. Journal of Alloys and Compounds, 2019, 775: 1147−1155.

[19] LUO Yin-yi, JIANG Xing-xing, YU Yan-jun, LIU Li-dan, LIN Xiang-tao, WANG Zhi-kai, HAN Lei, LUO Zhi-wei, LU An-xian. Enhancement of electrical properties of $LiTi_2(PO_4)_3$ ceramics via trivalent cation doping and microstructure regulation strategies [J]. Solid State Ionics, 2023, 390: 116111.

[20] WANG Zhi-yan, KOU Zhi-yan, MIAO Chang, XIAO Wei. Improved performance all-solid-state electrolytes with high compacted density of monodispersed spherical $Li_{1.3}Al_{0.3}Ti_{1.7}(PO_4)_3$ particles [J]. Ceramics International, 2019, 45: 14469−14473.

[21] LIU Xin-gang, TAN Jiang, FU Ju, YUAN Ruo-xin, WEN Hao, ZHANG Chu-hong. Facile synthesis of nanosized lithium-ion-conducting solid electrolyte $Li_{1.4}Al_{0.4}Ti_{1.6}(PO_4)_3$ and its mechanical nanocomposites with $LiMn_2O_4$ for enhanced cyclic performance in lithium-ion batteries [J]. ACS Applied Materials & Interfaces, 2017, 9(13): 11696−11703.

[22] MA Fu-rui, ZHAO Er-qing, ZHU Shao-yin, YAN Wen-chao, SUN De-ye, JIN Yong-cheng, NAN Ce-wen. Preparation and evaluation of high lithium ion conductivity $Li_{1.3}Al_{0.3}Ti_{1.7}(PO_4)_3$ solid electrolyte obtained using a new solution method [J]. Solid State Ionics, 2016, 295: 7−12.

[23] MA Qian-li, XU Qi, TSAI C L, TIETZ F, GUILLON O. A novel sol-gel method for large-scale production of nanopowders: Preparation of $Li_{1.5}Al_{0.5}Ti_{1.5}(PO_4)_3$ as an example [J]. Journal of the American Ceramic Society, 2016, 99(2): 410−414.

[24] WAETZIG K, ROST A, LANGKLOTZ U, MATTHEY B, SCHILM J. An explanation of the microcrack formation in $Li_{1.3}Al_{0.3}Ti_{1.7}(PO_4)_3$ ceramics [J]. Journal of the European Ceramic Society, 2016, 36(8): 1995−2001.

[25] YAMAI I, OTA T. Grain size-microcracking relation for $NaZr_2(PO_4)_3$ family ceramics [J]. Journal of the American Ceramic Society, 1993, 76(2): 487−491.

[26] ODA K, SAITOH H, HOAKI Y, SHIMODA H, HIRAO T, ICHIYOSHI W, TAKASE S, SHIMIZU Y. A lithium-ion conductive $Li_{1.5}Al_{0.25}Ga_{0.25}Ti_{1.5}(PO_4)_3$ solid electrolyte for electrochemical device [J]. Solid State Ionics, 2020, 346: 115212.

[27] HE Sheng-nan, XU You-long, ZHANG Bao-feng, SUN Xiao-fei, CHEN Yan-jun, JIN Yan-ling. Unique rhombus-like precursor for synthesis of $Li_{1.3}Al_{0.3}Ti_{1.7}(PO_4)_3$ solid electrolyte with high ionic conductivity [J]. Chemical Engineering Journal, 2018, 345: 483−491.

[28] ESAKA T, GREENBLATT M. Lithium ion conduction in substituted Li_5GaO_4 phases [J]. Solid State Lonics, 1986, 21(3): 255−261.

[29] WEN Zhao-yin, XU Xiao-xiong, LI Jing-xin. Preparation, microstructure and electrical properties of $Li_{1.4}Al_{0.4}Ti_{1.6}(PO_4)_3$ nanoceramics [J]. Journal of Electroceramics, 2009, 22: 342−345.

[30] LI Shui-xian SHANG Fei, WANG Yi, CHEN Guo-hua. Influences of ZrO_2 content on microstructural and ionic conductivity of $Li_{1.4}Al_{0.4}Ti_{1.6}(PO_4)_3$ solid-state electrolytes [J]. Solid State Ionics, 2024, 406: 116460.

[31] CAI Ze-hua, HUANG Yu, ZHU Wei-chen, XIAO Ren-gui. Increase in ionic conductivity of NASICON-type solid electrolyte $Li_{1.5}Al_{0.5}Ti_{1.5}(PO_4)_3$ by Nb_2O_5 doping [J]. Solid State Ionics, 2020, 354: 115399.

[32] WANG Qiao-hui, LIU Lei, ZHAO Bo-jie, ZHANG Lei, XIAO Xiao, YAN Hao, XU Guo-li, MA Lei, LIU Yong. Transport and interface characteristics of Te-doped NASICON solid electrolyte $Li_{1.3}Al_{0.3}Ti_{1.7}(PO_4)_3$ [J]. Electrochimica Acta, 2021, 399: 139367.

[33] YU Qi-peng, HAN Da, LU Qing-wen, HE Yan-bing, LI Song, LIU Qi, HAN Cui-ping, KANG Fei-yu, LI Bao-hua. Constructing effective interfaces for $Li_{1.5}Al_{0.5}Ge_{1.5}(PO_4)_3$ pellets to achieve room-temperature hybrid solid-state lithium metal batteries [J]. ACS Applied Materials & Interfaces, 2019, 11(10): 9911−9918.

[34] AONO H, SUGIMOTO E, SADAOKA Y, IMANAKA N, ADACHI G. Ionic conductivity of solid electrolytes based on lithium titanium phosphate [J]. Journal of the Electrochemical Society, 1990, 137: 1027.

[35] WEI Tong-ye, YANG Gong-zheng, WANG Chen-xin. Iso-oriented $NaTi_2(PO_4)_3$ mesocrystals as anode material for high-energy and long-durability sodium-ion capacitor [J]. ACS Applied Materials & Interfaces, 2017, 9(37): 31861−31870.

[36] TVERGAARD V, HUTCHINSON J W. Microcracking in ceramics induced by thermal expansion or elastic anisotropy [J]. Journal of the American Ceramic Society, 1988, 71(3): 157−166.

[37] XU Lin, TANG Sun, CHENG Yu, WANG Kang-yan, LIANG Ji-yuan, LIU Cui, CAO Yuan-cheng, WEI Feng, MAI Li-qiang. Interfaces in solid-state lithium batteries [J]. Joule, 2018, 2(10): 1991−2015.

烧结温度和保温时间对 $Li_{1.5}Ga_{0.5}Ti_{1.5}(PO_4)_3$ 快离子导体电解质结构和性能的影响

罗银易[1]，梁皓璋[1]，张 平[1]，韩 磊[2]，张 骞[2]，刘李丹[1]，罗志伟[1]，宁天翔[1]，卢安贤[1]

1. 中南大学 材料科学与工程学院，长沙 410083；
2. 江西理工大学 材料科学与工程学院，赣州 341000

摘 要：$Li_{1.5}Ga_{0.5}Ti_{1.5}(PO_4)_3$(LGTP)被认为是一种很有前途的锂离子固态电解质材料。在不同工艺条件下制备 LGTP 固体电解质材料，探讨烧结温度和保温时间对材料相对密度、相组成、微观结构、体积电导率和总电导率的影响。在阻抗测试频率 1~10^6 Hz 范围内，样品的体积电导率随烧结温度的升高而增加，总电导率先增加后降低。SEM 结果表明，晶粒大小受温度控制，平均晶粒尺寸从 750 ℃时的(0.54±0.01) μm 增大到 950 ℃时的(1.21±0.01) μm。随着孔隙率的增加，陶瓷样品的相对密度随温度升高而增加，然后降低。保温时间对晶粒尺寸增长或样品密度影响不大，但延长保温时间会导致裂纹产生，从而降低固体电解质的导电性。

关键词：烧结温度；保温时间；电导率；裂纹；固态电解质

(Edited by Xiang-qun LI)